

IMECE2003-42583

THE ACCELERATION OF MICRO-AND NANO-PARTICLES IN SUPERSONIC DE-LAVAL-TYPE NOZZLE

Tien-Chien Jen
 Mechanical Engineering Department
 University of Wisconsin, Milwaukee
 Milwaukee, WI 53211

**Longjian Li, Qinghua Chen, Wenzhi cui,
 Xinming Zhang**
 College of Power Engineering
 Chongqing University, Chongqing 400044
 China

ABSTRACT

The particle velocity in cold gas dynamic spraying (CGDS) is one of the most important factors that can determine the properties of the bonding to the substrate. The acceleration of gas to particles is strongly dependent on the densities of particles and the particle size. In this paper, the acceleration process of micro-scale and nano-scale copper (Cu) and platinum (Pt) particles in De-Laval-Type nozzle is investigated. A numerical simulation is performed for the gas-particle two phase flow with particle diameter ranging from 100nm to 50 μ m, which are accelerated by carrier gas Nitrogen in a supersonic De-Laval-type nozzle. The results show that cone-shape weak shocks (compression waves) occur at the exit of divergent section and the particle density has significant effect on the acceleration of micro-scale particles. At same inlet condition, the velocity of the smaller particles is larger than the larger particles at the exit of the divergent section of the nozzle.

NOMENCLATURE

A area[m²]
 A_p surface area of the particle [m²]
 c_p specific heat capacity [J/(kg.K)]
 C_{e1}, C_{e2}, C_m turbulent model constant
 D_p particle diameter[m]
 F_D drag force per unit particle mass[N/kg]
 h convective heat transfer coefficient [W/m²-K]
 k turbulent kinetic energy [m²/s²]
 m_p mass of the particle [kg]

p pressure [N/m²]
 Pr molecular Prantl number
 R ideal gas constant
 Re Reynolds number
 T temperature [K]
 T time [s]
 u_i velocity component in i-direction (i = 1,2,3) [m/s]
 x_i Cartesian coordinate in the i-direction (i = 1,2,3) [m]
Greek
 Γ thermal conductivity [W/(m.K)]
 ϵ dissipation ratio of turbulent kinetic energy [m²/s³]
 μ viscosity [kg/(ms)]
 μ_{eff} effective viscosity [kg/(ms)]
 ρ density of fluid [kg/m³]
 $\alpha_T, \alpha_k, \alpha_\epsilon$ inverse effective Prandtl number for energy equations, T , k and ϵ
Subscripts
i,j,k general spatial indices
eff turbulent effective parameters
mol molecule property
p particle property
t turbulent quantity

INTRODUCTION

The feasibility of a low temperature CGDS material deposition technology was demonstrated based on the introduction of 1- μm to 50- μm solid metal particles into a gas stream accelerated to supersonic velocities, and subsequently deposited on the substrate [1]. CGDS process has been considered as a promising new process to the well-established thermal spraying process. The deleterious effects of high temperature oxidation, evaporation, melting, crystallization, residual stresses, debonding and gas release can be avoided. Moreover, the advantages of this approach include the high bond strength of the particle, the high production rate due to the high deposition rate (deposition efficiencies of up to 80%), and the ability to recycle the powders.

Only a few works have been done on the simulation of CGDS particle acceleration process, moreover, current spraying particle size of the CGDS is usually more than 1 μm [1] [2] [4]. Dykhuizen and Smith [3] have modeled the gas dynamics of CGDS, using a one-dimensional flow model, and concluded that in order to increase the particle impact velocity, a longer nozzle, smaller

particles need to attain enough momentum. Therefore, for a certain material and a certain diameter of particles its velocity gained in supersonic nozzle must be greater than a critical velocity for a bond to form; below this critical velocity particle either bounce off the substrate or wear the substrate material. This critical velocity is approximately 450m/s for copper powder with 5 μm diameter impinging on copper substrate, as shown in McCune *et al.* [2].

To provide information on the development of velocity to smaller particles along the nozzle, we use the CFD program FLUENT to calculate the nitrogen carrier gas acceleration of copper and platinum particles with different diameters in a nozzle with a ratio of expansion of $A_E/A^* = 28.4$ illustrated in Figure 1. The calculations refer to copper and platinum particles with diameter from 100 nm to 50 μm , nitrogen as the process gas with an inlet pressure $p_0 = 2.0\text{ MPa}$ and a temperature $T_0 = 773\text{ K}$.

MATHEMATIC MODEL

The physical configuration of the nozzle is schematically shown

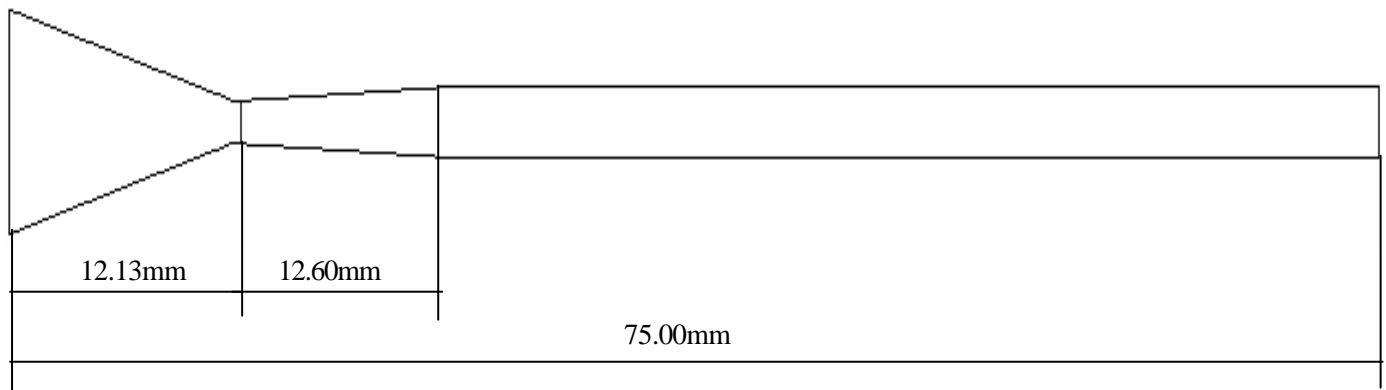


Figure 1 Schematic of the nozzle pipe

particles, higher operating pressure or a lower molecular weight carrier gas should be used. By using CFD (Computational Fluid Dynamics) program FLUENT Yen[5] used nitrogen and helium as carrier gases to simulate the acceleration process of copper powder diameter varying from 5 μm to 25 μm with the inlet conditions at $P_0 = 2.5\text{ MPa}$ and $T_0 = 673\text{ K}$.

In this study our primary intention is to extend CGDS technology to nano-scale particle size. If successful, this research can certainly open a door for more cross-disciplinary applications of nano- and CGDS technology such as cold surface coating technology. To develop this new nano-particle CGDS coating technology, we need to understand the details of nano-particles transport process in a supersonic gas. In order to bond powder particles to the substrate upon impact, the

in Figure 1. The geometries of the nozzle are exactly the same as that of the test nozzle in the experimental apparatus, which has been established in our experiment lab. The computation domain is composed of a De-Laval-Type (convergent-divergent) nozzle connected with a straight pipe, which is used to further accelerate the particle. The RNG $k-\epsilon$ model proposed by Yakhot and Orszag [6] is chosen for modeling the turbulent flow in the pipe. The RNG $k-\epsilon$ model was derived using a rigorous statistical technique (called renormalization group theory), which has an additional term in its ϵ equation that significantly improves the accuracy for rapidly strained flows. The feature makes the RNG $k-\epsilon$ model more accurate and reliable for a wider class of flows than the standard $k-\epsilon$ model. In the three-dimensional Cartesian coordinate system, the time-averaged

differential-governing equations for compressible flows of ideal gas are written in tensor form as follows:

mass

$$\frac{\partial (\rho u_i)}{\partial x_i} = 0 \quad (1)$$

momentum

$$\frac{\partial (\rho u_i u_j)}{\partial x_j} = \frac{\partial}{\partial x_j} \left[\mathbf{m}_{eff} \left(\frac{\partial u_i}{\partial x_j} + \frac{\partial u_j}{\partial x_i} \right) \right] - \frac{\partial p}{\partial x_i} \quad (2)$$

Energy:

$$\begin{aligned} \frac{\partial (\rho u_i c_p T)}{\partial x_i} &= \frac{\partial}{\partial x_i} \left[\mathbf{a}_T \left(\mathbf{m}_{eff} \frac{\partial T}{\partial x_i} \right) \right] \\ &+ \frac{\partial u_i}{\partial x_j} \left[\mathbf{m}_{eff} \left(\frac{\partial u_i}{\partial x_j} + \frac{\partial u_j}{\partial x_i} \right) - \frac{2}{3} \frac{\partial u_k}{\partial x_k} \right] \end{aligned} \quad (3)$$

Turbulent Kinetic Energy:

$$\begin{aligned} \frac{\partial (\rho u_i k)}{\partial x_i} &= \frac{\partial}{\partial x_i} \left[(\mathbf{a}_k \mathbf{m}_{eff} \frac{\partial k}{\partial x_i}) \right] \\ &+ \mathbf{m}_t S^2 - \rho \mathbf{e} \end{aligned} \quad (4)$$

Dissipation Rate of Turbulent Kinetic Energy:

$$\begin{aligned} \frac{\partial (\rho u_i \mathbf{e})}{\partial x_i} &= \frac{\partial}{\partial x_i} \left[(\mathbf{a}_e \mathbf{m}_{eff} \frac{\partial \mathbf{e}}{\partial x_i}) \right] \\ &+ C_{1e} \frac{\mathbf{e}}{k} \mathbf{m}_t S^2 - C_{2e} \rho \frac{\mathbf{e}^2}{k} - R \end{aligned} \quad (5)$$

For compressible flows, the ideal gas law is written in the following form:

$$p / \rho = RT \quad (6)$$

The effective viscosity \mathbf{m}_{eff} is calculated by the following equation:

$$\mathbf{m}_{eff} = \mathbf{m}_{mol} \left[1 + \sqrt{\frac{C_m}{\mathbf{m}_{mol}}} \frac{k}{\sqrt{\mathbf{e}}} \right]^2 \quad (7)$$

where \mathbf{m}_{mol} is the molecular viscosity. Equation (7) indicates that the RNG $k - \mathbf{e}$ model yields an accurate description of how

the effective turbulent transport varies with the effective Reynolds number (or eddy scale), allowing accurate extension of the model to low-Reynolds-number and near-wall flows. The coefficients \mathbf{a}_T , \mathbf{a}_k , and \mathbf{a}_e in Eqs. (3) – (5) are the inverse effective Prandtl numbers for T , k , and \mathbf{e} , respectively. They were computed using the following formula:

$$\frac{|\mathbf{a} - 1.3929|^{0.6321}}{|\mathbf{a}_0 - 1.3929|} \frac{|\mathbf{a} + 2.3929|^{0.3679}}{|\mathbf{a}_0 + 2.3929|} = \frac{\mathbf{m}_{mol}}{\mathbf{m}_{eff}} \quad (8)$$

Where \mathbf{a}_0 is equal to $1/\text{Pr}$, 1.0, and 1.0, for the computation of \mathbf{a}_T , \mathbf{a}_k , and \mathbf{a}_e , respectively. S in Eqs. (4) and (5) is the modulus of the mean rate-of-strain tensor, S_{ij} , which is defined as $S = \sqrt{2S_{ij}S_{ij}}$, where

$$S_{ij} = \frac{1}{2} \left(\frac{\partial u_i}{\partial x_j} + \frac{\partial u_j}{\partial x_i} \right). \quad R \text{ in Eq. (5) is given by}$$

$$R = \frac{C_m \rho \mathbf{h}^3 (1 - \mathbf{h} / \mathbf{h}_0) \cdot \mathbf{e}^2}{1 + \mathbf{z} \mathbf{h}^3} \cdot \frac{\mathbf{e}^2}{k} \quad (9)$$

where $\mathbf{h} = S \cdot k / \mathbf{e}$, $\eta_0 \approx 4.38$, $\mathbf{z} = 0.012$. The model constants C_m , C_{1e} , and C_{2e} are equal to 0.085, 1.42, and 1.68, respectively.

In the near wall zone, the two-layer-based, non-equilibrium wall function was used for the near-wall treatment flow in curved pipes. This method requires some consideration of mesh, i.e., the cell adjacent to the wall should be located to ensure that the parameter y^+ ($\equiv \rho u_\tau y / \mathbf{m}$) or y^* ($\equiv \frac{\rho C_m^{1/4} k_P^{1/2} y_P}{\mathbf{m}}$) falls into

the 30–60 range. In the present study, y^+ was adapted into the 30–60 range.

The particle is treated as discrete phase dispersed in the continuous phase, and the motion of which is computed using a Lagrangian formulation that includes the discrete phase inertia, hydrodynamic drag, and the force of gravity, heating of the discrete phase as well as the effects of turbulence on the dispersion of particles due to turbulent eddies present in the continuous phase. The trajectory of a discrete phase particle is predicted by integrating the force balance on the particle. This force balance equates the particle inertia with the forces acting on the particle, and can be written (for the x direction in Cartesian coordinates) as

$$\frac{du_p}{dt} = F_D(u - u_p) + g_x(\mathbf{r}_p - \mathbf{r}) / \mathbf{r}_p + F_x \quad (10)$$

where F_D is the drag force per unit particle mass, which is equivalent to $F_D = \frac{18\mu C_D \text{Re}}{r_p D_p^2}$. Here u is the fluid phase velocity, u_p is the particle velocity, μ is the molecular viscosity of the fluid, ρ is the fluid density, ρ_p is the density of the particle, and D_p is the particle diameter. Re is the relative Reynolds number (*i.e.* particle Reynolds number), which is defined as

$$\text{Re} = \frac{rD_p |u_p - u|}{\mu}$$

(11)

The drag coefficient C_D , can be taken from:

$$C_D = a_1 + \frac{a_2}{\text{Re}} + \frac{a_3}{\text{Re}^2} \quad (1)$$

2)

Here, a_1 , a_2 and a_3 are constants (see Appendix) that apply for smooth spherical particles over several ranges of Re given by Morsi and Alexander [7]. For sub-micron particles, a form of Stokes' drag law is available [8]. In this case, F_D is defined as $F_D = \frac{18\mu}{r_p D_p^2} C_c$. The factor C_c is the Cunningham correction

to Stokes' drag law:

$$C_c = 1 + \frac{2\lambda}{D_p} [1.25 + 0.4 \exp(-1.1(D_p / 2\lambda))] \quad (13)$$

where λ is the molecular mean free path. The third term on the right of Equation (10) incorporates additional forces (F_x) in the particle force balance. For sub-micron particles, the Brownian force and the Saffman's lift force [9] are taken into consideration. The effects of Brownian force and the Saffman's lift force are optionally included in the additional force term only in some special computation domain where the flow is Stokes flow.

In order to predict the dispersion of the particles due to turbulence, a stochastic method is used to determine the instantaneous gas velocity. In the stochastic tracking approach, the turbulent dispersion of particles is calculated by integrating the trajectory equations for individual particles, using the instantaneous fluid velocity, $u + u'$, along the particle path during the integration. The inert heating law is applied to account for the heat transfer between particle and gas phase. Due to the small size of the particle, a lumped capacitance method is used to relate the particle temperature, T_p , to the convective heat transfer and the absorption/emission of radiation at the particle surface,

$$m_p c_p \frac{dT_p}{dt} = hA_p (T_\infty - T_p) \quad (13)$$

Here, m_p represents the mass of the particle (kg), and C_p is the heat capacity of the particle (J/kg-K), A_p is the surface area of the particle (m^2), T_∞ is the local temperature of the continuous phase (K), and h is the combined convective and radiation heat transfer coefficient ($\text{W}/\text{m}^2\text{-K}$).

NUMERICAL COMPUTATION

The governing equations for the compressible flows and particle motion in the nozzle pipe are solved with a control-volume finite element method (CVFEM), incorporated in the software Fluent. The second-order upwinding scheme proposed by Rhie and Chow [10] was selected for the discretization of the convection term in the governing equations. A structured non-uniform grid system has been used to discretize the computation domain. For a compressible flow with weak shocks, the gradient adaption is used in **Fluent** for the solution of the supersonic flow. The pressure gradients in the solution are used to adapt the grid. The calculations continuing on the adapted grid result in a much sharper definition of the shocks. The grid independence was investigated in the analysis by adopting different grid distributions. The grid independence test indicated that the grid system of 150,000 ensured a satisfactory solution.

Based on the assumption that the particle phase is present at a low mass and momentum loading, in which the continuous phase is not impacted by the presence of the discrete phase, the two different phases can then be uncoupled to solve iteratively. This is a two-step procedure. First, the SIMPLE method is used to solve the continuous phase flow field. Then the particle trajectories for discrete phase of interest are calculated. In this paper, the flow medium is nitrogen (N_2), the particle phases is copper (Cu) and platinum (Pt), respectively.

RESULTS AND DISCUSSION

Figure 2 shows the isotaches of the N_2 carrier gas in the nozzle. It can be seen that the velocity reaches its maximum at the exit of the divergent section. At the location of the connection between the divergent section and the following straight section, the supersonic flow is forced to turn through a small angle. Therefore, cone-shape weak shocks (compression waves) occur, which results in the velocity fluctuating. The average velocity decreases considerably due to the friction in the straight section as shown in Figure 3. A comparison on the velocity distribution for the centerline velocity and the average velocity is also shown in Figure 3. It can be observed that the centerline velocity is essentially the same in the convergent section and most part of the divergent section of the flow channel. This is because the flow is highly turbulent, thus the

velocity distribution is very uniform as shown in Figure 2. However, near the exit of the divergent channel the deviation of the average velocity with the centerline velocity become

divergent section of nozzle, and then they decelerate with the carrier gas in the extended straight section. This reveals that shorter extended nozzle section is better when the particle

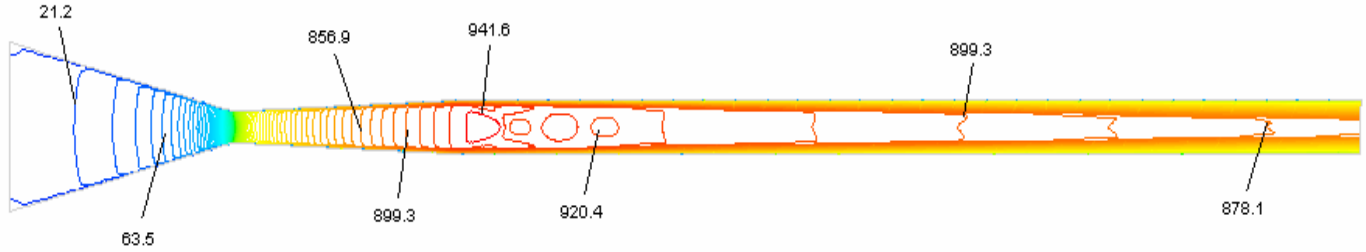


Figure 2 N₂ gas isotaches of in the nozzle

apparent. This is due the downstream cone-shape weak shocks affect the upstream velocity in the divergent channel, which causes the non-uniform velocity distribution in this region.

diameter is in nano-scale. The results also show that the extended straight section may have different optimal length for different size of the particles, and may be even unnecessary for

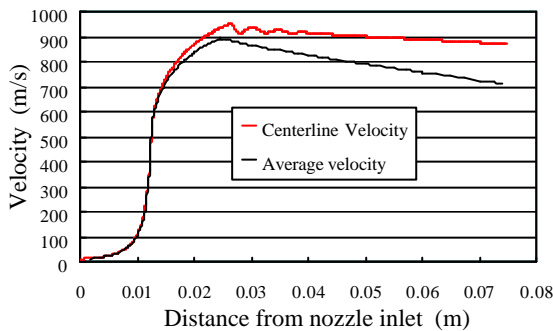


Figure 3 The average velocity and the centerline velocity of N₂ gas

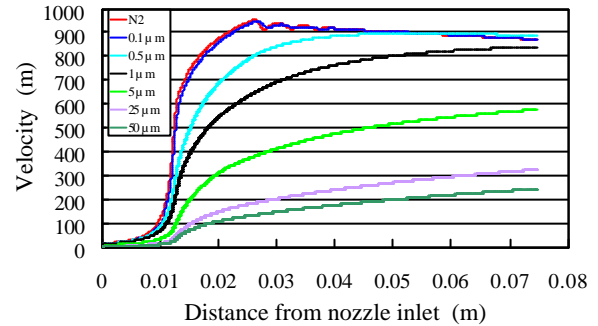


Figure 5 Velocity of platinum particles with different diameters

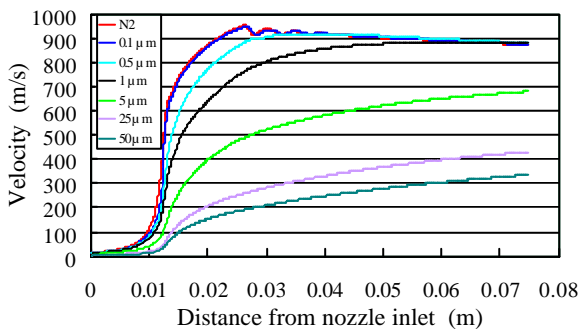


Figure 4 Velocity of copper particles with different diameters

Figures 4 and 5 depict the centerline velocity distribution along the axial direction for copper and platinum particles with different sizes. It can be seen from both figures that a longer nozzle, i.e. longer straight section, can further accelerate larger particles to higher velocity. However, for smaller particles, for example the nano-scale particle diameters (e.g., 0.1 μm or 100nm), their velocities approach the carrier gas velocity at the exit of

nano-size particle, which is strikingly different than the previous investigations.

Figure 6 compares the particle centerline velocities of copper and platinum with same diameter of 5 μm and 0.1 μm. It is clearly observed that the densities of particles have significant effect to the acceleration of bigger particles. Higher density

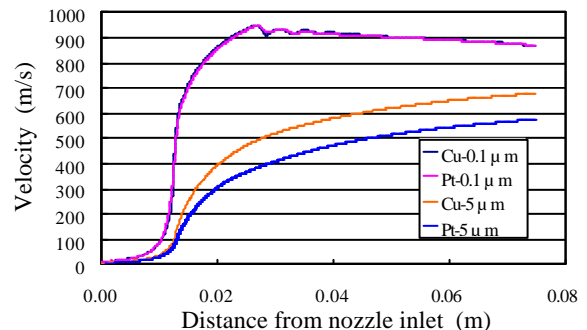


Figure 6 The velocity comparison of copper and platinum particle with same diameters

particle (Pt) has a smaller acceleration in the nozzle due to its larger mass, and the lighter particle (Cu) accelerates fast due to its smaller mass. Nevertheless, this effect almost disappears when the particle size decreases to 0.1 μ m (100nm) diameter. Therefore, in order to accelerate particles of 0.1 μ m diameter or smaller size to a much higher velocity, the nozzle inlet gas pressure (and temperature) is required to increase to a much higher value or other complemented acceleration approaches (e.g., electric field or magnetic field) have to be used to increase the particle velocity.

CONCLUSIONS

1. A small turn angle at the location of the connection between the divergent section and the following straight section caused cone-shape weak shocks (compression waves), which results in the velocity fluctuating in the straight section of nozzle.
2. The friction in the straight section causes the average velocity of carrier gas decreases considerably.
3. A longer nozzle (i.e. longer straight section) is useful only to the acceleration of bigger particles (micron size). To reach higher velocity, an optimized length can be obtained for different particle sizes.
4. The particle density has significant effect to the acceleration of bigger particles (micron size); nevertheless, this effect disappears to smaller particles of 0.1 μ m (100nm) diameter.
5. For nano-scale particles, the much higher nozzle inlet gas parameters (pressure and temperature) are required to reach higher exit velocities.

APPENDIX

The drag coefficient equation (12) used are

$$C_D = \frac{24.0}{Re}$$

for $Re < 0.1$,

$$C_D = 3.69 + \frac{22.73}{Re} + \frac{0.0903}{Re^2}$$

for $0.1 < Re < 1$,

$$C_D = 1.222 + \frac{29.1667}{Re} - \frac{3.8889}{Re^2}$$

for $1 < Re < 10.0$,

$$C_D = 0.6167 + \frac{46.5}{Re} - \frac{116.67}{Re^2}$$

for $10.0 < Re < 100.0$,

$$C_D = 0.3644 + \frac{98.33}{Re} - \frac{2778}{Re^2}$$

for $100.0 < Re < 1000.0$,

$$C_D = 0.357 + \frac{148.62}{Re} - \frac{4.75 \times 10^4}{Re^2}$$

for $1000.0 < Re < 5000.0$,

$$C_D = 0.46 - \frac{490.546}{Re} + \frac{57.87 \times 10^4}{Re^2}$$

for $5000.0 < Re < 10000.0$,

$$C_D = 0.5191 - \frac{1662.5}{Re} + \frac{5.4167 \times 10^6}{Re^2}$$

for $10000.0 < Re < 50000.0$,

ACKNOWLEDGEMENT

The authors, Qinghua Chen and Longjian Lee, acknowledge the support of this work by China National Natural Science Foundation Grant No. 50276073

REFERENCES

- [1] Alknimov, A.P., Kosarev, V.F. and Apayrin, A.N. (1990). "A Method of Cold Gas Dynamic Deposition." Dokl Acad. Nauk SSSR (318) 1062-1065.
- [2] McCune, R. C., Papyrin, A. N., Hall, J. N., Riggs, W. L. and Zajchowski, P. H., "An Exploration of the Cold Gas Dynamic Spray Method for Several Materials Systems," Proc. 8th National Thermal Spray Conf., Houston, Texas, pp. 1-5, 1995.
- [3] Dykhuizen, R. C. and Smith, M. F., "Gas Dynamic Principles of Cold Spray," Journal of Thermal Spray Technology, Vol. 7, Number 2, pp. 205-212, 1998.
- [4] McCune, R. C., Donlon, W. T., Cartwright, E. L., Papyrin, A. N., Rybicki, E. F. and Shadley, J. R., "Characterization of Copper and Steel Coatings Made by the Cold Gas Dynamic Spray Method," Proc. 9th National Thermal Spray Conf., Cincinnati, pp.

397-403, 1996.

- [5] Yap Yik Yen, <http://rat.liv.ac.uk/research/cgdm>
- [6] Yakhot, V., and Orszag, S. A., "Renormalization Group Analysis of Turbulence: I. Basic Theory," J. Scientific Computing, 1(1), pp.1-51, 1986.
- [7] Morsi, S. A. and Alexander, A. J., "An Investigation of Particle Trajectories in Two-Phase Flow Systems", J. Fluid Mech., Vol.55, No.2, pp193--208, 1972.
- [8] Ounis, H., Ahmadi, G. and McLaughlin, J. B., "Brownian Diffusion of Submicrometer Particles in the Viscous Sublayer" Journal of Colloid and Interface Science, Vol.143, No.1, pp.266--277, 1991.
- [9] Li, A. and Ahmadi, G., "Dispersion and Deposition of Spherical Particles from Point Sources in a Turbulent Channel Flow", Aerosol Science and Technology, Vol.16, pp.209-226, 1992.
- [10] Rhie, R. M., and Chow, W. L., "Numerical Study of the Turbulent Flow Past an Airfoil with Trailing Edge Separation.", AIAA Journal, Vol.21, No.11, pp.1525-1532, 1983.